Univerza *v Ljubljani*
Fakulteta za *matematiko in fiziko*

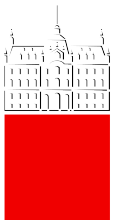

Oddelek za fiziko

Seminar I_b

1^{st} year, 2^{nd} cycle

Drops impacting on a surface

Author: Matic Knap
Mentor: prof. dr. Rudolf Podgornik

Ljubljana, March 2015

Abstract

In our seminar we present the dynamics of drops impacting on a solid surface. Firstly we describe the methods for capturing the impact of drop on solid surface. Further on we describe essential role of the air trapped between the impacting drop theoretically and experimentally.

Contents

1 Introduction

There's no doubt that you have been outside in the rain watching little drops of water splashing on lake or a car window. Drops impacting on a surface is a well known phenomena but quite complex to fully understand. Since 1908 when Worthington [1] started to study drops impacting on surface he wanted to attract researchers from other fields, not only to explain phenomena, but also because of its importance in technological applications. Most stunning and beautiful splashing patterns that occur are explained by rapid impact followed by shock wave as the fluid bounces back the surface, seen on Figure 1a. Those splashes have been recorded by high-speed camera pioneer Harold E. Edgerton. His image of milk drop coronet is one of the most famous pictures of modern art and science.

(a) Deep pool of milk splash [10].

(b) Flat surface splash.

Figure 1: Figure 1a shows splash on deep pool of water, caused by water drop. Figure 1b is splash on flat solid surface.

As previously mentioned splashes are not just beautiful to observe, they're also present in many technological and scientific fields:

- drop impact at spray cooling, fuel injection, ink-jet printing or spray painting,

- thin coatings on surfaces,
- erosion in steam turbines caused by high-speed impacts with solids,
- splashed pesticide droplets can be blown away by wind and pollute neighboring areas,
- splashing rain drops provide mechanism for dispersal of fungus spores,
- in forensics the study of patterns of impacted blood drops can be significant in reconstructing crimes.

Droplets impacting on surfaces have two major points of view, impacting a deep pool of liquid or impacting a solid surface. Those two views are divided in two categories:

- those where velocity is above threshold for splash occurrence,
- and those below threshold velocity.

Studying drops impacting on a deep pool of liquid is more complex than studying droplets impacting on flat solid surface, because surface of deep pool of liquid is deformed before and after the impact.
That's why in our seminar we focused on drops falling on a flat solid surface with velocities below splash threshold velocities.

2 Skating on a film of air

Dynamics of free drops failing from height on surface is well known, but near impact there are still some missing explanations of phenomena that occurs. Before the contact of drop with the surface can occur, the drop must first drain the air separating it from the surface. There is no doubt that at reduced ambient pressure, splash is reduced. It has been proved by many experiments trough history. Therefore the air separating solid and liquid may be far greater importance as we think. Recent theoretical calculation suggest that, even at moderate impact velocities the air fails to drain and is instead compressed, deforming and flattening the bottom of the drop while serving as a thin cushion of air a few tens of nanometers thick to lubricate spread of the drop and leading to eventual formation of a trapped bubble of air within the drop [4]. With new experimental methods they are able to measure contact dynamics of a drop impacting on a dry glass surface [3]. They directly observed a thin film of air that initially separates the liquid from the surface enabling much more rapid lateral spreading of the drop providing striking confirmation of the theoretical predictions. There are three main techniques used combined to observe a thin film of air. For lower impact velocities is used total internal reflection (TIR) microscopy combined with virtual frame technique (TIR) [2]. Larger impact velocities are observed with photodiode operating at 100 MHz.

2.1 TIR measurements

To observe the thin film of air, the top surface of a dove prism is illuminated with a collimated light source, at an angle of incidence greater than the angle for total internal

reflection (TIR) of the glass-air interface and lesser than the angle of total internal reflection of the glass-liquid isopropanol interface. Exponentially decaying evanescent field forms above the reflecting surface. The characteristic decay length of the evanescent field depends on the wavelength of the light, the indices of refraction of the glass and air, and the incidence angle. The incidence angle is typically 45 degrees, corresponding to a characteristic decay length 100 nm. The light is recorded on the camera's imaging sensor after it reflects off of the surface of the prism, resulting in a point-wise intensity measurement, $I(x, y, t)$.

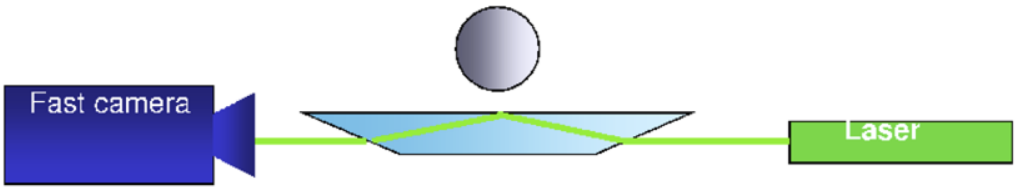

Figure 2: Schematics of TIR microscopy [2].

As the droplet enters the evanescent field, less light is reflected, and the liquid appears as a gray scale on the camera's imaging sensor. This directly probes the thin layer of air. There is a region in the image that routinely captures a multiply reflected beam, directly above the impact center as viewed in the images recorded by the camera's imaging sensor. The reflected light is recorded using a high speed camera, with images captured at rates up to 150000 frames per second, with a minimal exposure time of 1 s. The recorded intensity is mapped to height using the following relationship:

$$h(x, y, t) = -\delta \log\left(1 - \frac{I(x, y, t)}{I(x, y, 0)}\right), \tag{1}$$

where $I(x, y, 0)$ is the intensity before the droplet enters the evanescent field. Normalizing $I(x, y, t)$ by $I(x, y, 0)$ subtracts the background and improves the signal to noise ratio.

2.2 Virtual frame technique

In many cases, even everyday phenomena occur over time scales too rapid to be captured by even the fastest high speed camera. Examples of this are numerous and include. The impact, breakup and coalescence of fluid droplets, dynamic fractures and electrical discharge of gasses. To overcome the inherent limitations of the frame rate of the fastest high speed cameras is used a completely new imaging method, virtual frame technique (VFT). VFT enables real time visualization of many such systems using a standard camera. Moreover, unlike conventional fast cameras that require a compromise between spatial resolution and speed, with VFT, the full spatial resolution of the camera is preserved. To use VFT, the visualization setup must first be adapted to produce an approximately binary signal. This can be achieved in many different ways. TIR results in nearly binary contrast between wetted and un-wetted surface, changing from completely bright to completely dark as soon as liquid-solid contact occurs. Also, a propagating crack front

can be translated into a binary signal by imaging the silhouette of an opaque material against a brightly lit background.

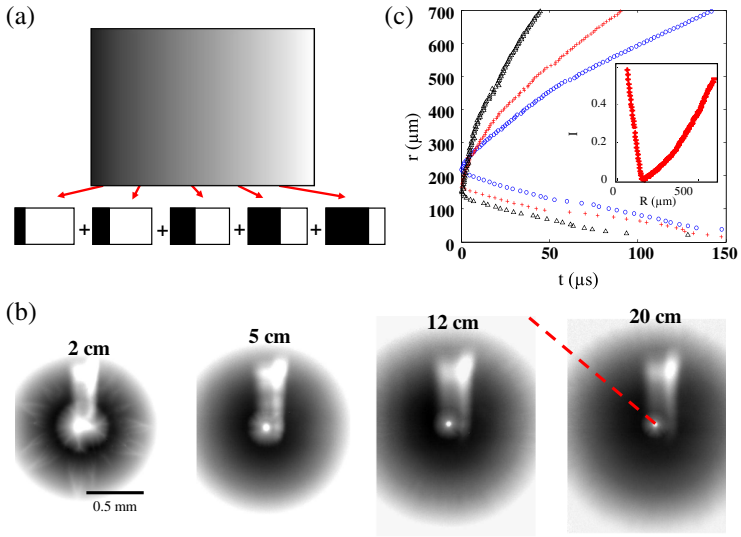

Figure 3: Virtual frame technique. a) schematic demonstrating the concept. Individual binary images, below, are integrated to yield the total gray-scale image. The gray scale can be interpreted to yield the time evolution. (b) Four VFT images taken at different values of H. Each image exhibits a square-shaped whiter region through the top center resulting from spurious reflections in the beam path; they are ignored in our analysis. (c) The intensity is converted to time and azimuthally averaged around the impact center. The distance of the wetting fronts from the center are plotted as a function of time for three typical experiments with $H = 26,\ 126,\ 456\ mm$ for blue circles, red pluses and black triangles, respectively [2].

VFT exploits this binary contrast by increasing the camera exposure time to integrate over times longer than the characteristic dynamics under the strict assumption that the dynamics remain irreversible within the integration time, thus ensuring that the intensity at any given position directly reflects the total time until the signal was switched from 0 to 1 (or 1 to 0). Thus, all pixels of equal gray-scale value are in fact isochrones, and consecutive binary contrast thresholds provide what is essentially a series of virtual frames capturing the entire dynamics. The assumption that once intensity at a pixel is switched from 0 to 1 (or 1 to 0) it will remain that constant for the remainder of the integration time is essential and guaranties that intensity can be uniquely mapped to time. The temporal resolution of the acquisition is set by the dynamic range of the camera and for some imaging sensors can be further improved by exploiting the gamma correction, which alters the exponent of the sensor response function; for a decelerating dynamics, gamma can be set to a value smaller than one, so that the temporal resolution is initially highest. Ideal applications of VFT include phenomena requiring temporal resolution in the 1-100 MHz range, for which the salient dynamics are irreversibly progressing fronts.

2.3 Photodiode measurements

For high-velocity drop impacts (velocities greater than 1 m/s), the dynamics of the air film dewetting the surface occur too rapidly to be regularly observed with the high speed camera. However, the air film formation occasionally occurs during the microsecond exposure of the camera, confirming its existence. In order to measure the dynamics of the air layer, the full-frame imaging of the camera is supplemented with an ultra-fast, single-point intensity measurement, recorded with a photodiode. The photodiode and camera are in conjunction with a cube beam splitter: half of the intensity is recorded on the camera's imaging sensor, while a portion of the remaining half of the intensity is sampled by the photodiode, as shown in the schematic in Figure 4

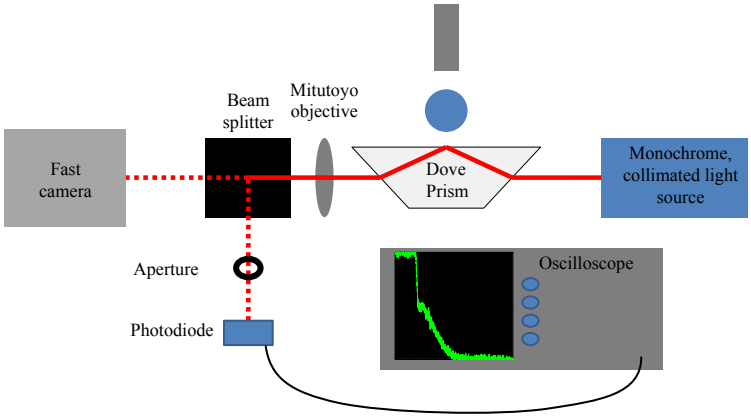

Figure 4: A schematic of the experimental set-up for the photodiode measurement. A beam splitter divides the intensity of the reflected light after it exits the prism, such that half of the light is imaged on the camera's sensor, and a portion of the remaining half of the intensity is sampled by the photodiode at up to 100 MHz. The remaining portion sampled by the photodiode can be restricted with an aperture. The intensity trace is recorded with an oscilloscope, which is set to trigger at a threshold intensity [2].

Intensity trace is recorded with an oscilloscope, which is set to trigger at a threshold intensity. The position and size of the area sampled by the photodiode relative to the camera's imaging sensor is precisely identified to within 4 microns by scanning a point probe over the interface. Two such photodiode locations are illustrated by colored circles in 5. Images shown correspond to the impact of a drop released from $H = 21\ cm$. The second frame clearly shows that even at these high impact velocities, a transient film is formed prior to contact. The actual area sampled by the photodiode depends on the magnification of the objectives we use (5x to 20x) as well as the opening of an adjustable aperture behind the objective. The diameter of the sampled area for the 10x objective used for all experiments shown, is 60 cm. In our setup, there is an unavoidable variability in the location of the impact center, which for drops falling from $H = 21\ cm$ is approximately 500 nm. However, the variability in the impact location provides a convenient means of probing the dynamics of the spatially extended air layer with the added temporal resolution of the photodiode without the need to displace the diode. We dropped hundreds of drops from $H = 21\ cm$, and recorded the intensity traces as well as

individual frames from the camera. In these data, there were several experiments that were ideally positioned to accurately measure the first moments of impact beneath and around the rim of the central air pocket with the photodiode; additionally, an occasional snapshot of the air layer was also captured in the image sequence, as shown in the second frame of Figure 5.

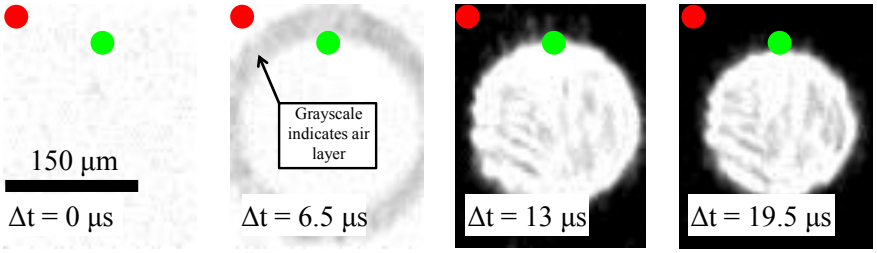

Figure 5: (a) A sequence of images recorded at 150000 frames-per-second with one μs exposure time for $H = 21\ cm$, including circles illustrating the locations probed by the photodiode: the first location, indicated by a green circle, is located partly beneath the dimple and partly beneath the initially developed air layer. The second location, shown in red, is entirely outside the immediate vicinity of the dimple. Notably, a $50\mu m$ x $25nm$ air layer is directly visualized in the second frame of the image sequence.

3 Mathematical model

We consider a droplet of radius R approaching a solid surface with velocity V. Close to surface, viscous and pressure forces in the gas decelerate the droplet, deforming the interface. This can be described by coupling flow in an incompressible, inviscid liquid cylinder to a gas layer underneath. Parameters describing the system include the viscosity of the gas μ_g, the liquid density ρ_l, the liquid surface tension σ_l and the state of gas. With compressible lubrication approximation [11] the gas film between solid and liquid deforms according to

$$12\mu_g(\rho_g h)_t = (\rho_g h^3 p_x)_x. \tag{2}$$

The equation for the droplet balances the acceleration of the liquid interface with the vertical pressure gradient: $\rho_l h_{tt} = -p_y^{liquid}$. The liquid pressure is related to the gas pressure using the Gibb's condition

$$p^{liquid} = p^{gas} + \sigma_l h_{xx} \tag{3}$$

We can relate p_y to p_x [12] resulting in the equation

$$\rho_l h_{tt} = \mathcal{H}[p_x + \sigma_l h_{xxx}] \tag{4}$$

where $\mathcal{H}$ is the Hilbert transform. We focus on the initial stages of impact, when the droplet first deforms from its spherical shape. Figure 6 shows subsequent snapshots in time of the interfacial and pressure profiles. The firs snapshot is when the parabola first begins to deform away from its uniform curvature state. Later snapshots show clearly the deformation of drop at height from the solid surface which stay roughly constant. To

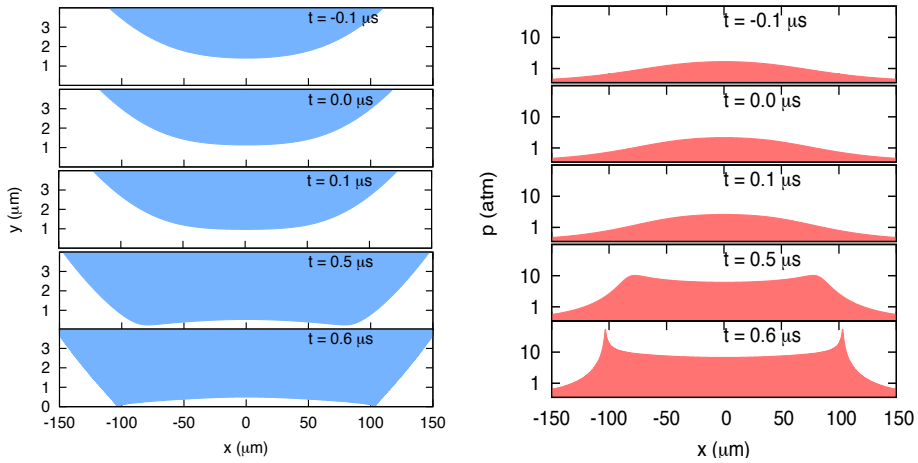

Figure 6: Snapshots from simulations documenting the deformation of a droplet before contacting the solid surface. Time is measured relative to the moment of contact if no gaseous layer were present. Over timescales of 0.1 μs, left panel shows deformations in the interface of the droplet occurring on the scales of μ m. Depending on impact, fluid and gas parameters, we demonstrate that further phenomena set in when the gas gap is of order $\sim$ 10 nm. Right panel shows the build up of the gas pressure as the minimum gap thickness decreases [13].

determine the height we must find the conditions of deformation. For droplet to deform, the pressure in the gas must be sufficient to decelerate the falling liquid from velocity V to rest. The gas pressure must balance the inertial pressure in the droplet. Owing to its parabolic shape, the approaching droplet, in interaction with the gas layer below, sets up a flow over a horizontal length scale $L = \sqrt{RH}$ in the gas. When the drop is far from the substrate, and the gas pressure is set by incompressible viscous drainage the equation 2 then implies $P \sim \mu_g V R/H^2$. Assuming sufficiently weak surface tension, the gas pressure gradient balances the liquid deceleration. This give us the height:

$$H_* = RSt^{2/3}, \tag{5}$$

where $St = \frac{\mu_g}{\rho_l V R}$ is the Stokes number. If the pressure in the gas becomes of order the ambient pressure before the drop can deform, the underlying gas compresses. This happens when $P_g \sim P_0$ or when critical height $H_* = R\sqrt{\mu_g V/RP_0}$. This critical height marks the transition from incompressible dynamics to a compressible one. To calculate H_* as a function of the height H from which the drop is released, we start from 5, given in terms of the initial drop height $V = \sqrt{2gH}$. Substituting the expression for H_* from equation 5 into $L = \sqrt{RH_*}$, we obtain

$$L = H^{-1/6} \frac{\sqrt[3]{12\mu_g R^2}}{(\rho_l^{1/3}(2g)^{1/6})} \tag{6}$$

The speed V, at which the fluid spread above a thin film of air can be estimated from a simple scaling analysis. The horizontal length scale L, divided by time scale of the

impact, $\tau \sim \left(\frac{R\mu_g^2}{\sqrt{2gH^5}\rho^2}\right)^{1/3}$ gives us a scale for the spreading velocity V to be

$$V = 0.34\left(\frac{\rho_l R(2gH)^2}{\mu_g}\right)^{1/3} \tag{7}$$

4 Confirmation of air layer

To visualize the contact dynamics we take a cut trough VFT and TIR recorded image at the location shown by the dashed red line in Figure 7a. Then convert the measured intensity to separation, and plot the time evolution, using color to denote the height as shown in Figure 7b.

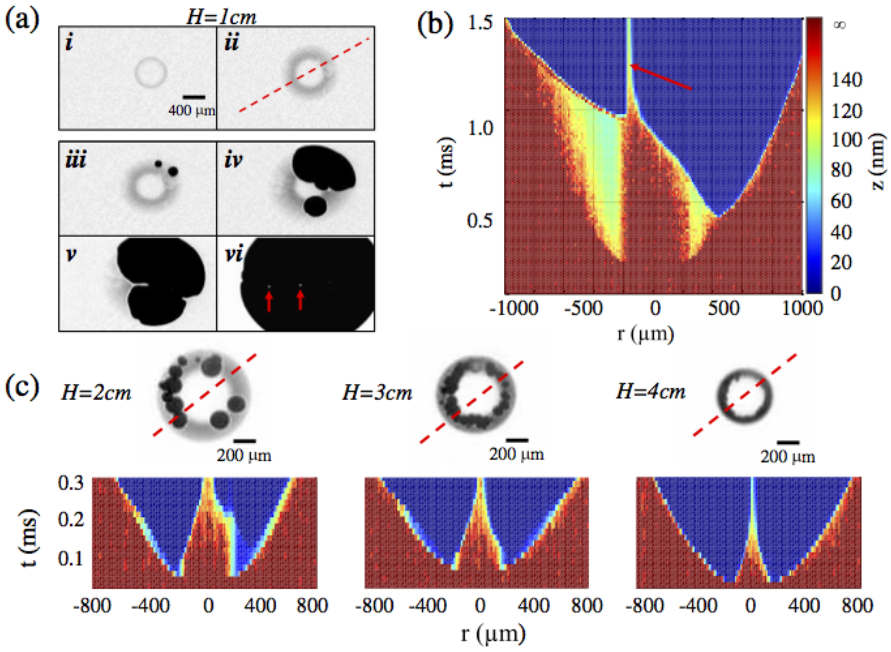

Figure 7: The behavior of the thin air film separating the impacting drop from the surface. a): six snapshots of a drop, released from $H = 1\ m$ illustrating the film of air and the impact dynamics. b): the impact dynamics along the cut shown by the dashed line in Figure 7a(ii). The height is indicated by the color. The arrow indicates one of the bubbles that remains trapped in the liquid [2].

As seen on the Figure 7b the first 500 μm clearly show the formation of the layer of air as the drop spreads before the liquid contacts the surface. The liquid does not spread inward, as seen by the boundaries of the thin film, denoted by the central region. This reflects the pocket of air which ultimately becomes a bubble trapped in the drop. While the layer of air is clearly responsible for decelerating the drop, it cannot retain the separation of the fluid and surface indefinitely. Ultimately, the thin film of air becomes unstable and contact occurs. Initially, two small dark spots appear in the film when the liquid fully contacts the surface, as shown on Figure 7a. As these spots grow, other spots appear, as the film of air breaks down. These liquid wetting fronts spread rapidly, wetting

the surface at a velocity of $\approx 1.5\ m/s$, comparable to that of the liquid spreading on the thin film of air. Interestingly, there is a thin line of air at the front of the spreading fluid where the air film becomes thicker as the air is pushed by the advancing wetting front, shown by the white region leading the edge of the black wetting front.

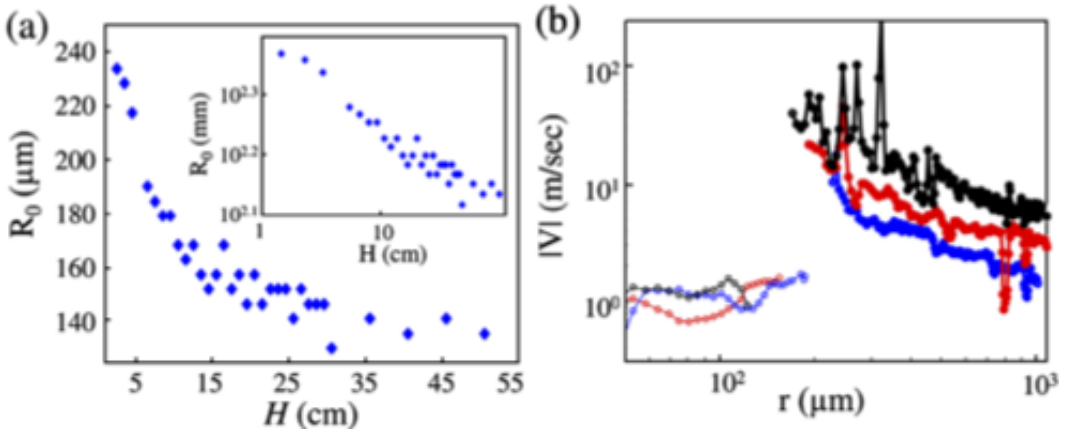

Figure 8: The initial dynamics of the wetting. Figure 8a: R_0, as a function of height (inset) same as main figure in log scale. Figure 8b: The inward (solid circles) and outward (open circles) velocity of the spreading liquid for different heights $H = 26, 126, 456\ mm$ [2].

To explore the initial dynamics of the wetting associated with the rupture or breakdown of the air cushion, the local instantaneous velocity is numerically calculated and plotted as a function of radial position r. The inward-moving velocity is constant, propagating at approximately $1.3\ m/s$. The outward-moving velocity decreases as $1/r$, and can exhibit remarkably high values, as large as $70\ m/s$, as shown in Figure 8b. Surprisingly, the velocity of the inward-moving front is independent of height H the drop is released. The maximum velocity of the outward moving front increases strongly with H, as shown on Figure 9a. Moreover, the maximum velocity of the outward-moving front is nearly an order of magnitude greater than the capillary velocity for isopropanol. When contact line advances, it must flow on very small scales to maintain contact with interface. Flow on these small scales is dominated by viscous dissipation and thus, the propagation rates are limited by the liquid capillary velocity. By contrast the velocities measured here are much larger. This suggest that the fluid is not in contact with the surface but is instead spreading on a thin film of air. Thus, the very early viscous dissipation is in the gas as it is squeezed out from under the liquid that wets the surface at an accelerated rate. Indeed such high velocities are predicted theoretically, but only with explicit assumption that the spreading occurs over a film of air, as indicated by the excellent agreement between the calculated behavior, shown by the solid line, and the data in Figure 9a. The intensity initially drops rapidly, corresponding to the passage of the liquid over the area sampled by the photo diode - the steep slope of the intensity drop is indicative of the very high speed at which the liquid spreads. However, the intensity does not drop all the way to zero, but instead levels off, reaching a plateau at a value $I/I_0 \approx 0.1$, where I_0 is normalization intensity before drop hits the interface. This intensity decreases to zero after

approximately 5 μs as shown in enlarged data set in Figure 9b and depends on height at which droplet was dropped. This plateau directly reflects the existence of the thin film of air that separates the liquid from the surface. The nature of the final decay of this plateau differs from experiment to experiment.

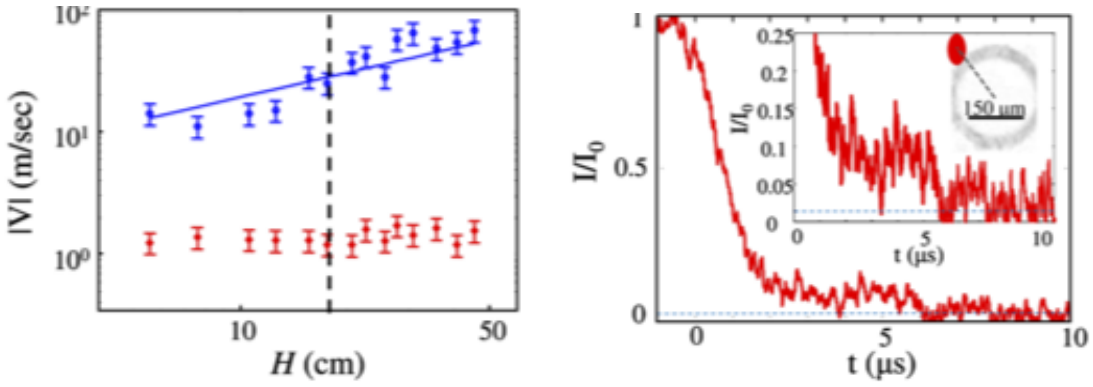

(a) (b)

Figure 9: The initial dynamics of the wetting. Figure 9a represents peak velocities for the outward (blue dots) and inward (red dots) fronts. Blue line is theoretically predicted initial outward spreading velocity [2]. The dashed line indicates the threshold height above which splash is observed. Figure 9b intensity of the reflected light directly underneath the thin air film at a location marked by a red spot in the inset for height 21 cm. Closeup of low intensity region. The image shown is a direct visualization of the thin film of air separating the liquid from the surface prior to contact [2].

Measurements on Figure 9b directly confirm the spreading of the liquid on a thin film of air of order 10 nm thick. This is trailed closely by a wetting front that rapidly expands due to the breakdown of the air film. Experimental results seen on Figure 9b directly demonstrates the existence of a thin film of air over which the liquid spreads. This provides confirmation of the theoretical prediction [4, 5] that a drop is skating on thin film of air until it breaks down. In addition those results reveal that qualitatively new phenomena occur as the thin film of air becomes unstable simultaneously breaking down at many discrete locations leading to wetting patches that grow and coalescence to fully wet the surface. Similar dynamics has also been reported to occur when a sheet of fluid is ejected as a drops splash after high velocity impact [6, 7]. For a perfectly wetting fluid such as isopropanol on a glass, a thin film of air behaves as does a poor solvent - it cannot remain stable and van der Waals forces will cause it to dewet the surface trough a nucleation or spinodal-like process. Initially, as height is increased, the air film becomes thinner, and the breakup of the air film occurs more rapidly. Thus, even though the rate of initial drop spreading increases with height, the length over which the drop skates on the air film decreases. However, as height increases still further, the thickness of the air film saturates, and hence the rate of breakup also saturates. The rate of initial spreading of the drop continues to increase with height. Thus, the drop always can skate over the film of air, even as height continues to increase. Interestingly, this skating on the film of air can persist, even until height increases enough that a sheet of fluid is ejected near the

expanding rim, and a splash is produced.

5 Conclusion

We have overview-ed the phenomena of drop impacting on surface which is not fully understood. Trough research, there were some visualization techniques discovered which captures falling drop from below rather than from the side. Results of experiment [2] have proven that qualitatively new phenomena occur as the thin film of air becomes unstable and dewets trough spinodal-like process. The rate at which contact occurs strongly depends on drop release height respectively on air film thickness. Moreover the drop always skate on film of air even if height is increased enough that splash is produced.We can conclude those experiments are highly important for drop splashing which has significant importance in wide palette of applications, such as ink-jet printing, turbine corrosion, or even to determine minimal plant placement to prevent disease spreading with splashing raindrops.

6 Bibliography

[1] Worthington A.M., *A Study of Splashes.*, Longmans, Green, and Co. (1908).

[2] Kolinski J.M., Rubinstein S.M., Mandre S., Brenner M.P., Weitz D.A., Mahadevan L., *Physical Review Letters Phys.* **108**, 074503 (2012).

[3] Rubinstein S.M., Cohen G., and Fineberg J., *Nature* (London) **430**, 1005 (2004).

[4] Mani M., Mandre S., and Brenner M.P., *J. Fluid Mech.*, **647**, 163 (2010).

[5] Mandre S., Mani M., and Brenner M.P., *Phys. Rev. Lett.*, **102**, 134502 (2009).

[6] Driscoll M.M, Stevens C.S., and Nagel S.R., *Phys. Rev. E*, **82**, 036302 (2010).

[7] Thoroddsen S.T., Takehara K., and Etoh T.G., *Phys. Fluids.*, **22**, 051701 (2010).

[8] De Gennes P.G, Brochard-Wyart F. , and Quere D., *Capillarity and Wetting Phenomena: Drops, Bubbles, Pearls, Waves*, (Springer Verlag, New York, 2004).

[9] Cahn J.W., *On spinodal decomposition*, Acta Met., **Vol. 9**, (1961).

[10] *http://www.agallery.com/pages/photographers/edgerton.html*, 14. March 2015.

[11] Taylor G. I and Saffman P. G., *J. Aeronaut. Sci.*, **24**, 553 (1957).

[12] Smith F., Li L., and Wu G., *J. Fluid Mech* , **482**, 291 (2003).

[13] Mani M., Mandre S. and Brenner M., *J. Fluid Mech.*, **647**, 163 (2010).